East European Journal of Physics. 3. 370-379 (2023)
DOI:10.26565/2312-4334-2023-3-39 ISSN 2312-4334

IMPACT OF CRYSTALLITE SIZE ON STRUCTURAL, OPTICAL AND MAGNETIC CHARACTERISTICS OF $La_{0.7}Sr_{0.15}Ca_{0.15}MnO_3$ NANOCRYSTALLINE†

Mohd Abdul Shukur[a,b], Katrapally Vijaya Kumar[a,*], Gade Narsinga Rao[c]
[a]*Department of Physics, JNTUH University College of Engineering Rajanna Siricilla, Agraharam, Rajanna Siricilla District, 505302, Telangana, India*
[b]*Department of Physics, SRR Government Arts & Science College (Autonomous), Karimnagar, 505001, Telangana, India*
[c]*Department of Physics. Marri Laxman Reddy Institute of Technology and Management, Dundigal, Hyderabad, Telangana, India*
**Corresponding Author e-mail: kvkphd@gmail.com, kvkumar@jntuh.ac.in*
Received May 20, 2023; revised June 30, 2023; accepted July 1, 2023

Nanocrystalline $La_{0.7}Sr_{0.15}Ca_{0.15}MnO_3$ (LSCMO) manganites were prepared by the combustion process and heated to various annealing temperatures (T_A) to get various sized crystallites. The X-ray diffraction (XRD) patterns provided evidence that a Rhombohedral structure with space group $R\bar{3}c$ was formed. Additionally, an increase in the size of the crystallites was observed, from 15.64 to 36.78nm, as the temperature (T_A) increased from 700°C to 1300°C. The FESEM micrographs revealed that homogeneous with porosity. The FTIR spectra showed five absorption peaks. The Optical energy gap of LSCMO nanocrystalline is decreased from 3.51 to 3.28 eV as annealed temperature raised, reveals that the LSCMO nanoparticles are semiconductor in nature. Room temperature Raman spectra of LSCMO nanoparticles demonstrate a notable reliance on annealing temperature. When the Raman modes were analysed with respect to T_A, it was observed that the Raman vibrational phonon mode below 200cm^{-1} (A_{1g}) and four modes (E_g) in the range 200-800cm^{-1} displayed significant displacements and widening, which were associated with oxygen sublattice distortion. Considerable changes were observed in both the intensity and full width half maximum (FWHM) of the five Raman modes as the annealing temperature increased. Magnetic behaviour using M-H loop at room temperature were measured by the Vibrating sample magnetometer revealed that gradation of saturation magnetization as the function of annealing temperature. Hence there is a remarkable crystallite size effect on optical and magnetic properties of LSCMO nanocrystallites.
Keywords: *Crystallite size; Optical band gap; FTIR spectra; M-H loop; Raman vibrational phonons*
PACS: 61.46. +w; 75.50. Gg; 7840.-q; 78.30.-j

INTRODUCTION

Colossal magnetoresistance (CMR) materials are a highly important research topic in the scientific field due to their exceptional properties in terms of structure, optical, and magnetism when compared to ordinary magnetic materials. These materials have a wide range of applications, including magnetic recording, flash memory technologies, hyperthermia, bioimaging, biosensor applications, and designing of semiconductor devices. Additionally, they can be utilized to create cooling systems that are highly efficient in terms of cooling while being environmentally friendly, producing minimal noise, and emitting no greenhouse gases [1,2].

Lanthanum doped perovskite manganite oxides with divalent alkaline earth ion substitution display interesting properties such as drastically change of electrical resistance with the magnetic field response, which is called as colossal magnetoresistance (CMR) and metal to insulating behaviour [3-7]. Substituting a divalent ion into La sites causes Mn^{+3} ions to transform into Mn^{+4}, resulting in magnetic exchange (Double Exchange) arises between Mn^{+3} and Mn^{+4} ions having in different oxidation states with electronic configurations of ($3d^4$, $t^3_{2g}\uparrow e^1_g\uparrow$, S=2) and ($3d^3$, $t^3_{2g}\uparrow e^0_g\uparrow$, S=3/2) respectively. The double exchange consequences the materials, whether they are ferromagnetic, antiferromagnetic or shows spiral magnetism. The magnetic properties of perovskite manganites are significantly influenced by the Mn+3/Mn+4 ratio, Mn-O bond length, and Mn-O-Mn bond angles, as they impact the double exchange interaction [8]. This behaviour can be altered through the introduction of suitable ions at A and B sites, resulting in a significant change in the characteristic behaviour of these manganites [9-14]. The method of preparation, magnitude, orientation of the unit cell, dopant, etc., all have an impact on the structural features of manganites. [15-17]. Manganite's transport and magnetic properties are affected by their crystalline size [18,19]. The size of the grains can be impacted by the annealing temperature, hence raising the T_A should result in the growth of the grains. [20,21]. The MI transition in $La_{1-x}Sr_xMnO_3$ can be attributed to the double exchange (DE) interaction, which explains the high bandwidth [22,25]. Similarly, the DE mechanism explains the small bandwidth of Metal Insulator transition and colossal magneto-resistance effect in $La_{1-x}Ca_xMnO_3$[26,27]. Perovskite-type manganites doped with lanthanum are fascinating materials with unique characteristics that make them highly sought after. To gain a thorough understanding of the complex properties of rare-earth manganites, it is essential to examine the interrelationship between their structural, optical, and magnetic properties. As electronic devices become increasingly integrated and miniaturized, these perovskite manganites are being produced at the nanoscale level. In recent years, research on perovskite manganites with nanoscale particle sizes has expanded significantly, driven by their intriguing properties, such as a significant ratio between surface area and volume and surface effects. Different

† ***Cite as:*** M.A. Shukur, K.V. Kumar, G.N. Rao, East Eur. J. Phys. 3, 370 (2023), https://doi.org/10.26565/2312-4334-2023-3-39

optical and magnetic properties are obtained by combining $La_{1-x}Sr_xMnO_3$ with La_{1-x} Ca_xMnO_3 in the appropriate ratio. Calcium doped Strontium – Lanthanum manganite exhibit remarkable properties as a high magnetocaloric material among divalent ions [28]. Raman spectroscopy is a widely recognized method that employs vibrational state data to offer insights into the chemical and structural properties of various compounds. The Raman spectra of La0.7Ca0.15Sr0.15MnO3 can provide insight into its vibrational modes, which are related to the material's structure and properties. The spectra would display peaks at different wavenumbers corresponding to the different vibrational modes of the material. Compared to bulk materials, nanoscale manganites exhibit novel characteristics that vary with particle size. Among several investigations using $La_{1-x}Sr_xMnO_3$ and La_{1-x} Ca_xMnO_3 only a handful had revealed coexisting Ca and Sr systems.

In this study, the combustion preparation method was employed to create La0.7Sr0.15Ca0.15MnO3 (LSCMO) nanoparticles due to its affordability, convenience, and ability to produce nanocrystals at modest annealing temperatures. Additionally, this method enables the production of LSCMO nanoparticles in large quantities, down to a few tenths of a gram. Various analytical tools were utilized to examine the structural, optical, and magnetic properties of the LSCMO nanoparticles, and the results showed that these nanocrystals exhibited typical properties.

EXPERIMENTAL

We prepared $La_{0.7}$ $Sr_{0.15}Ca_{0.15}MnO_3$ (LSCMO) nanocrystallites using high-purity nitrate precursors of $La(NO_3)_3.6H_2O$, $Sr(NO_3)_2$,$Ca(NO_3)_2.4H_2O$ and $Mn(NO_3)_2.4H_2O$.The nitrate compounds were dissolved in de-ionised water based on their stoichiometry and mixed to form a precursor solution. To this solution, citric acid ($C_6H_8O_7$) was added in a 1:3 molar ratio to the total moles of nitrate ions. The solution was stirred continuously until a white precipitate was formed. Ammonia was then gradually added neutralize the pH of 7, resulting in a thick, brown solution. The mixture was then heated at 60°C with continuous stirring for three hours, and ethylene glycol was added. The gelation agent was ethylene glycol, and the chelating agent was citric acid. The resulting solution was heated at 100°C until it turned into a gel, and then heated to 300°C until it was completely burned, resulting in a free dark powder [29]. The powder was then finely ground and divided into four parts, each of which was annealed separately at 700, 900, 1100, and 1300°C (sample code LSCMO7, LSCMO9, LSCMO11, LSCMO13) for four hours to produce nanocrystallites of various sizes.

The crystal structure, crystallite size, and phase identification of LSCMO nanocrystalline were identified using the X-ray powder diffraction method with CuKα (λ = 1.5418Å) radiation using a Rigaku (Miniflex-II) diffractometer with 0.02°step size. Field Emission Scanning Electron Microscopy (FESEM) (CARLZESIS - Ultra 55) and Energy Dispersive Spectroscopy (EDS) (OXFORD-INCAx-act) were used to evaluate the surface morphology, nanostructure, and elemental composition. Fourier transform infrared spectroscopy (FTIR) (SHIMADU), UV-Vis spectroscopy (SYSTRONICS DOUBLE BEAM), and Raman spectrometry (Lab RAM HR, HORIBA, France) were used to assess the optical characteristics. The resolution of the FTIR measurements, which ranged from 400 to 4000cm^{-1}, was 4cm^{-1}. To acquire the optical absorbances, ultrasonic assisted dispersing of a small quantity of sample in distilled water was performed, and the data was captured in the range of 100-800nm. Raman spectroscopic studies were carried out using laser light of λ = 532nm as the 1% illumination source with 1cm^{-1} resolution, and the slit was adjusted to obtain data in the range of 100-800nm.

RESULT AND DISCUSSION

XRD, FESEM and EDS Analysis

In Figure 1, the X-ray powder diffraction (XRD) pattern of LSCMO7, LSCMO9, LSCMO11, and LSCMO13 nanocrystallites at room temperature is presented. The JCPDS# 51-0409 and Rietveld by Full Prof software were used to match the XRD patterns as shown in the Figure 2, confirming the formation of pure and single-phase Rhombohedral structure with space group $R\bar{3}c$. The intensity of the prominent peak observed at around 32.8° for LSCMO13 perovskite structure was substantially higher than that of the other samples, which can be attributed to the large crystalline size and high electron density.

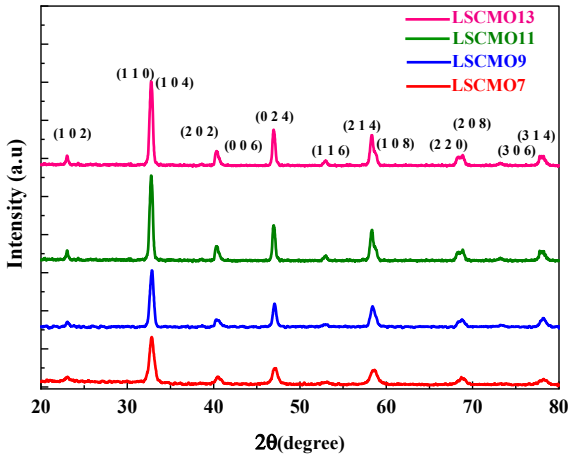

Figure 1. X-ray diffraction patterns of LSCMO7, LSCMO9, LSCMO11, and LSCMO13 nanocrystallites

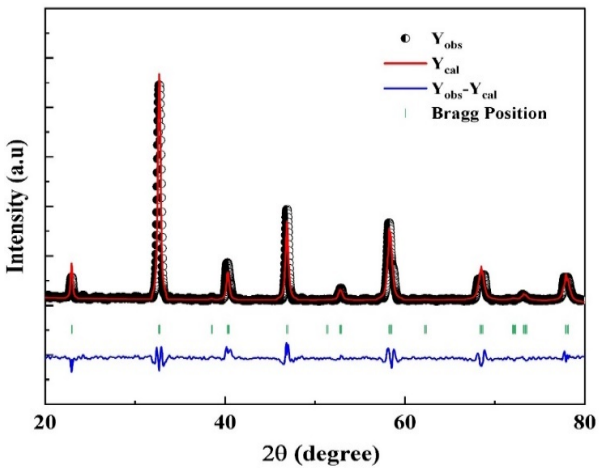

Figure 2. Rietveld refinement of LSCMO13 nanocrystallite

The average crystallite size $\langle D \rangle$ relates to full width half maximum of Bragg's peaks at different annealing temperatures were calculated using Scherrer formula (1) [30].

$$\langle D \rangle = \frac{K\lambda}{\beta \cos\theta} \quad (1)$$

Where K is the shape factor which is equal to 0.9.

It was observed that average crystallite size values were increased from 15.64 to 36.78 nm as a function of T_A which were shown in Figure 3. The structural parameters and crystallite sizes are depicted in Table 1.

FESEM images of the prepared LSCMO7, LSCMO9, LSCMO11, and LSCMO13 samples were shown in Figure 4. The fluffy nature and voids powder can be ascribed to the significant amount of gases released during the reaction. The average particle size changed from 42.23 nm to 327.5 nm as the annealing temperature was increased. The particles seemed to be cluster together with no apparent shape at low annealing temperature. The crystal grains entirely solidified at 1100 and 1300°C, generating homogeneous and independent nanoparticles. Better crystalline structure and very well symmetry were reported at 1300°C. as a result, from the morphological studies, the crystal growths were consistent with the XRD data.

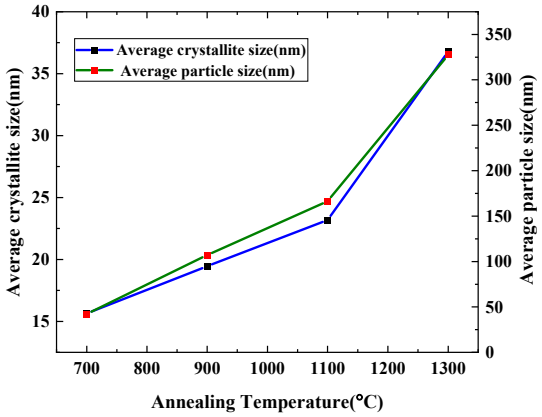

Figure 3. Variation of Crystallite Size as function of Annealing temperature of LSCMO7, LSCMO9, LSCMO11, and LSCMO13 nanocrystallites

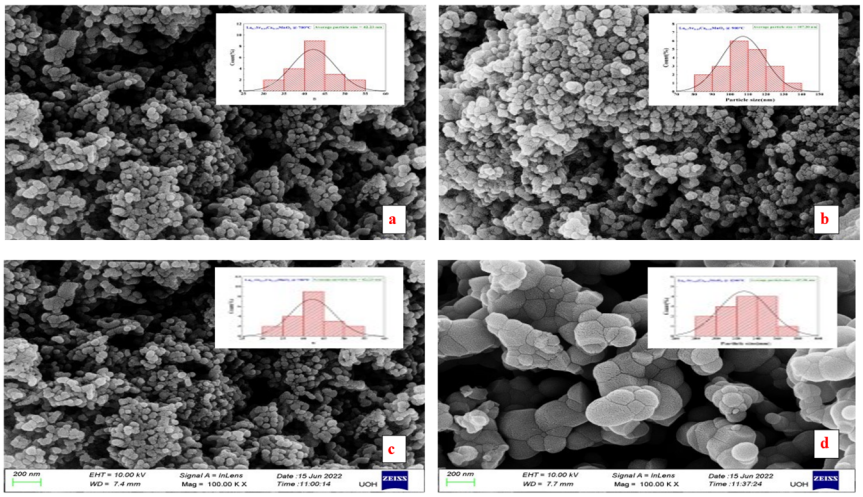

Figure 4. FESEM micrographs of (a) LSCMO7, (b) LSCMO9, (c) LSCMO11, and (d) LSCMO13 nanocrystallites

Table 1. Structural parameters of LSCMO7, LSCMO9, LSCMO11, and LSCMO13 nanocrystallites

Sample code	**LSCMO7**	**LSCMO9**	**LSCMO11**	**LSCMO13**
Lattice Parameter (a, b) (nm)	0.54764	0.54896	0.54935	0.55944
Lattice Parameter (c) (nm)	1.33502	1.33333	1.33395	1.3442
Volume of Unit Cell ($Å^3$)	346.74	347.98	348.81	348.93
Crystallite Size D (nm)	15.64	19.46	23.18	36.78
Average particle size(nm)	42.23	107.20	166.44	327.5

To better understand the distribution of individual surface elements, EDX analysis of post annealed samples were illustrated the results in Figure 5 and atomic percentages of individual elements were Table 2. The EDX revealed the uniform distribution concerned elements on the nanostructure surfaces. This accurately depicts the stoichiometric quantities utilized in the experiment.

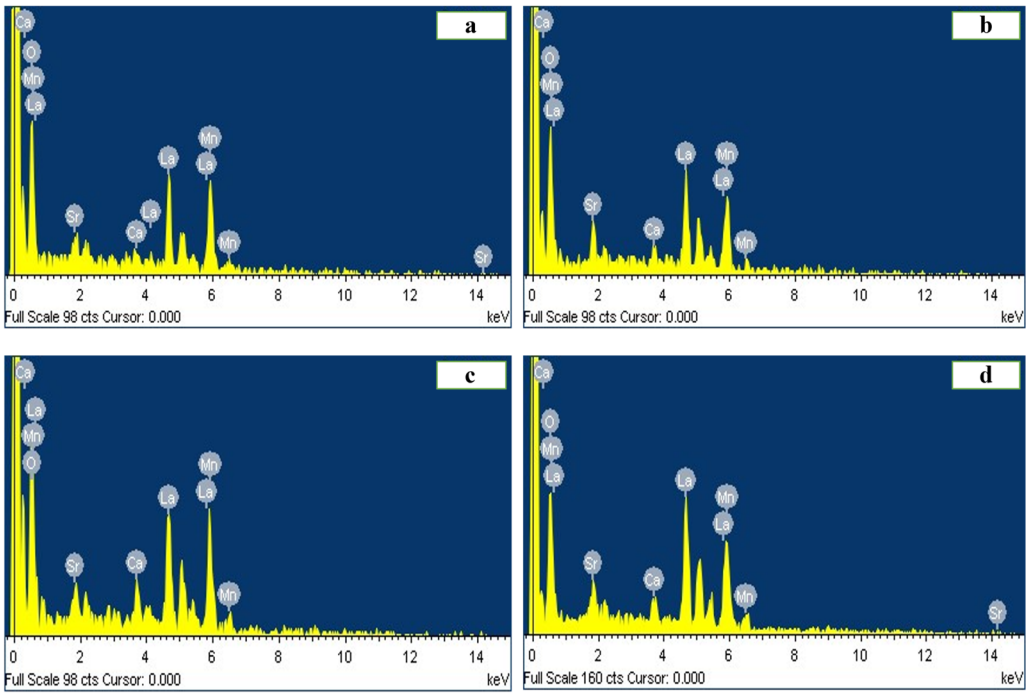

Figure 5. EDX patterns of (a) LSCMO7, (b) LSCMO9, (c) LSCMO11, and (d) LSCMO13 nanocrystallites

Table 2. Atomic percentage of LSCMO7, LSCMO9, LSCMO11, and LSCMO13 nanocrystallites from EDX.

Sample code	La	Sr	Ca	Mn	O
LSCMO7	14.75	1.83	1.79	21.53	60.1
LSCMO9	16.11	3.84	2.31	17.93	59.81
LSCMO11	13.04	1.66	3.4	18.88	63.02
LSCMO13	21.04	2.28	3.12	20.78	52.78

FTIR Spectra Analysis

The lattice phonon vibrations of LSCMO7, LSCMO9, LSCMO11, and LSCMO13 after annealing were analyzed using Fourier Transform Infrared (FTIR) spectroscopy and shown in the Figure 6.

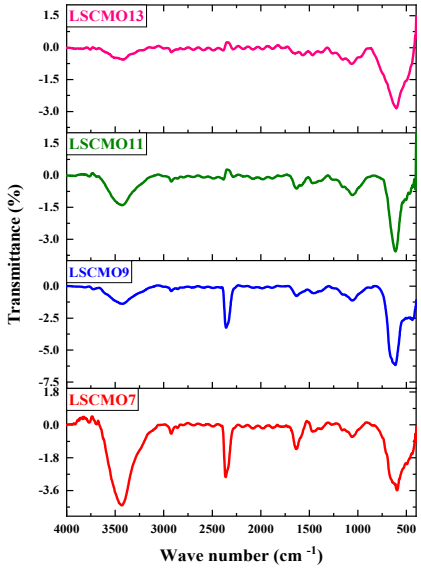

Figure 6. FTIR patterns of LSCMO7, LSCMO9, LSCMO11, and LSCMO13 nanocrystallites

Mn-O bond stretching vibration mode was observed in all the prepared LSCMO samples, which was attributed to the JT effect, and a strong absorption peak was seen at 597cm^{-1}[31]. The stretching vibration mode frequency of metal-oxygen bond shifted towards high wave numbers (blue shift) as the annealing temperature increased to 1300°C, indicating additional deformation of the MnO_6 octahedron [32]. The absorption peak at 1059cm^{-1} confirmed the presence of carbonate and decreased with increasing annealing temperature [33]. The C=O bond symmetric stretching vibration peak around 1631cm^{-1} and the C=C bond antisymmetric stretching vibration peak at 1360cm^{-1} also decreased with increasing annealing temperature. [34,35]. The O-H stretching vibration mode was confirmed by the wide band observed at 3600cm^{-1}, which originated from the ethylene glycol solvent used in nanoparticle synthesis [34]. LSCMO13 showed less intense peaks at 1059, 1360, 1631, and 3600cm^{-1} due to weak vibrations, indicating the formation of pure crystallinity. The presence of stretching and bending modes in the transmission spectra confirmed the formation of the LSCMO perovskite structure, which was consistent with the XRD results.

UV-Vis Spectroscopic Analysis

The optical characteristics of LSCMO7, LSCMO9, LSCMO11, and LSCMO13 nanocrystals are defined by their energy gap and refractive index as the main physical features. To investigate these properties, UV-Vis absorption spectroscopy was conducted on the prepared samples and variation of absorption peaks with wavelength were shown in Figure 7. A clear absorption edge was observed in the ultraviolet to visible range, with wavelengths ranging from 447 to 468nm for all samples.

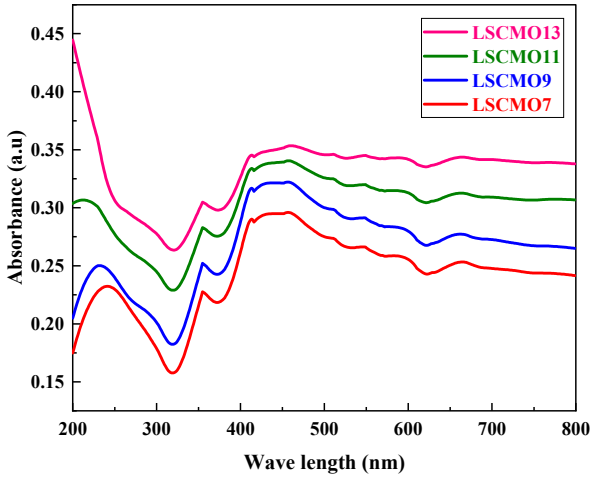

Figure 7. UV-Vis absorbance spectra of LSCMO7, LSCMO9, LSCMO11, and LSCMO13 nanocrystallites

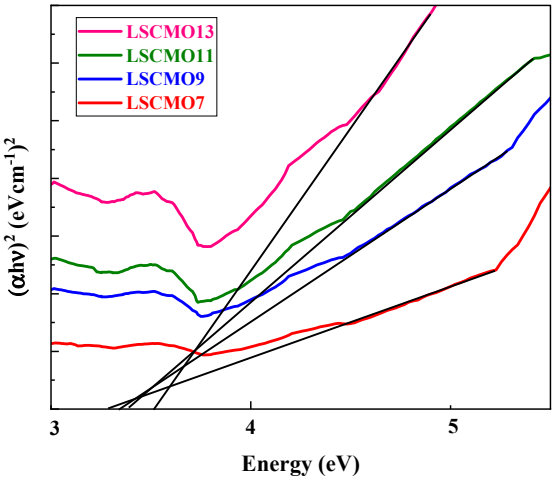

Figure 8. UV-Vis absorbance -Tauc plot: Variation of $(\alpha h\nu)^2$ versus photon energy "hν" of LSCMO7, LSCMO9, LSCMO11, and LSCMO13 nanocrystallites

The absorption coefficient (α) was calculated using equations (2), (3), and (4) [36,37].

$$I = I_0 e^{\propto t} \tag{2}$$

$$A = log \frac{I_0}{I} \tag{3}$$

$$\alpha = \frac{2.303\ A}{t} \tag{4}$$

where 'A' and 't' are the absorbance and thickness of sample respectively.

The band gap of LSCMO7, LSCMO9, LSCMO11, and LSCMO13 nanocrystallites was determined using Tauc's relation (5) and resulting Tauc plots [38].

$$(\alpha h\nu)^n = A(h\nu - E_g) \tag{5}$$

Equation (5) relates the band gap (E_g), frequency (ν), and refractive index (n) to the absorption coefficient (α), Planck's constant (h), and photon energy (hν). Different values of n (1/2, 1, 3/2, and 2) were used to plot $(\alpha h\nu)^n$ against photon energy. Variation of $(\alpha h\nu)^2$ versus photon energy "hν" of LSCMO7, LSCMO9, LSCMO11, and LSCMO13 nanocrystallites is shown Figure 8 and a linear relationship was observed over a wide range of energy, indicating a direct transition from higher to lower energy levels. The optical bandgap values for LSCMO7, LSCMO9, LSCMO11, and LSCMO13 nanocrystallites were obtained by extending the linear section of the graph on the 'hν' axis. These values, presented in Table 3, show that the optical band gap decreases from 3.51 eV to 3.28 eV with increasing annealing temperature (T_A), due to increase in crystallite size as confirmed by XRD analysis. These results suggest that the prepared nanocrystallites may be useful in photocatalytic applications based on their band gap energy values [39].

Table 3. Optical parameters of LSCMO7, LSCMO9, LSCMO11, and LSCMO13 nanocrystallites

Sample code	**LSCMO7**	**LSCMO9**	**LSCMO11**	**LSCMO13**
Absorption peak(nm)	447.2	448.7	448.9	468.8
Band gap (eV)	3.51	3.39	3.34	3.28
Refractive Index (By Moss Relation)	2.2680	2.2776	2.2974	2.3128
Refractive Index (By Herve and Vandamme)	2.2074	2.2396	2.2520	2.2682
Static dielectric constant (ε_o)	7.4628	7.6476	8.0172	8.2944
High frequency dielectric constant (ε_α)	5.1438	5.1874	5.2780	5.3490

The refractive index of prepared LSCMO nanoparticles were measured by Moss relation (6) as well as Herve and Vandamme relation (7) [40-43].

$$E_g n^4 = 95eV \tag{6}$$

$$n = \sqrt{1 + \left(\frac{A}{E_g + B}\right)^2} \tag{7}$$

A=13 .6 eV, B=3.4eV represents the hydrogen ionization energy constants. The static dielectric constant (ε_o) and high frequency dielectric constant (ε_α) of all samples are determined using the following relation (8) and (9) [44].

$$\varepsilon_o = 18.52 - 3.08E_g \tag{8}$$

$$\varepsilon_\alpha = n^2 \tag{9}$$

The theoretically measured values of n, ε_o, ε_α for LSCMO7, LSCMO9, LSCMO11, and LSCMO13 were posted in Table 3, reveals that the refractive index rises as the annealing temperature rises and rate of rise appears to be depending on the models utilized. The static dielectric constant (ε_o) and high frequency dielectric constant (ε_α) were also increased with T_A.

Raman Spectroscopic Analysis

Several recent articles have argued that optical properties of perovskite type manganites were affected by "the Mn-O bond length and symmetry of MnO_6, which establishing the link between the optical phonon mode and Jahn Teller mode" [45]. The Jahn-Teller effect impacts on the rhombohedral structure of manganite. In this structure, the dynamic and incoherent distortion of MnO_6 is influenced by six identical Mn-O bond lengths. Despite this distorted configuration, only five Raman-active modes related to the vibration and stretching of oxygen vibrations of MnO6 can typically be observed [46,47]. $La_{0.7}$ $Sr_{0.3}MnO_3$ nanocrystallites possess a rhombohedral structure with space group $D_{3d}^6(R\bar{3}c)$ and Jahn-Teller phenomenon is a crucial factor in controlling "the dynamic and non-coherent deformation of MnO_6". In the rhombohedral distorted structure, only five Raman-active modes ($1A_{1g} + 4E_g$) can be observed, which are associated with MnO_6 vibrations and stretching oxygen vibrations [46]. Among these modes, two ($1A_{1g} + 1E_g$) "correspond to rotational or tilt stretching mode, while one Eg mode is associated with the bending mode. The other two E_g modes are related to the anti-stretching of the MnO6 octahedra and the vibration of A ions" [48]. "Previous studies have indicated that the Raman spectra of La0.7 Sr0.3MnO3 nanoparticles exhibit two weak modes at 180 and 425cm-1, with the former being an A_{1g} symmetry mode associated with an out-of-phase rotation, and the latter being an Eg symmetry mode related to the bending mode of the MnO6 octahedra" [49].

The Raman spectra at room temperature of LSCMO7, LSCMO9, LSCMO11, and LSCMO13 nanocrystallites were obtained in the spectrum of wave number 50-1500 cm^{-1} and presented in Figure 9, shows that five vibration modes were observed in the range 100-800cm^{-1} for the all the samples, which correspond to the phonons of the rhombohedral structure with space group D_{3d}^6 , $Z = 2$. "This particular structure can be derived from a simple cubic perovskite by rotating the neighbouring MnO_6 octahedra in opposite directions along the$[111]_c$ cubic direction"[50].

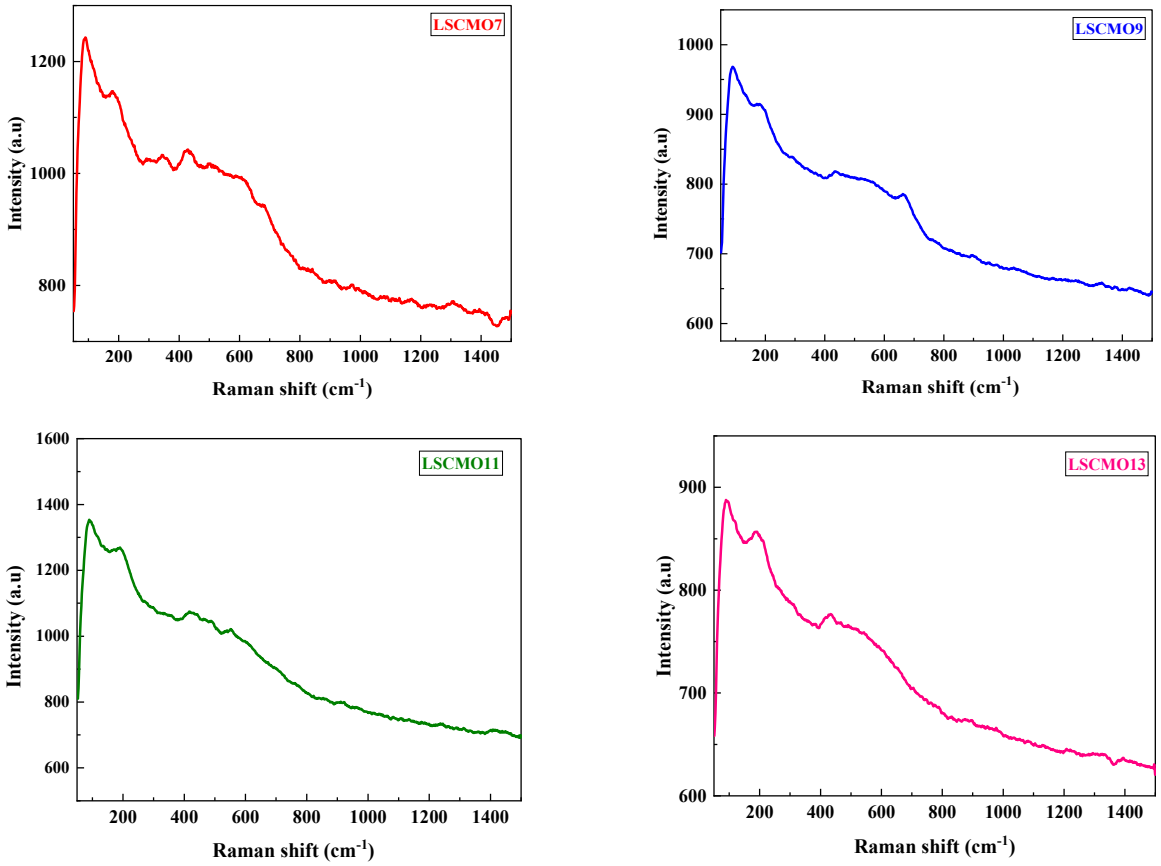

Figure 9. Room temperature Raman spectrum of LSCMO7, LSCMO9, LSCMO11, and LSCMO13 nanocrystallites

The position of peaks in the Raman spectra can be identified clearly by deconvolution of peaks using by the Lorentz fitting, and five vibration modes were observed for all samples, which were shown in the Figure 10.

The positions of vibration modes of LSCMO7, LSCMO9, LSCMO11, and LSCMO13 nanocrystallites were shown in Table 4. The vibration mode at lower frequencies occurs around 177, 184, 189, and 190 cm^{-1} for LSCMO7, LSCMO9, LSCMO11, and LSCMO13 nanocrystallites respectively, which shows. The A_{1g} phonon mode is associated with the primary distortion of A-site cations (such as La, Sr, Na, or Ca) and the strength of the electron-phonon coupling [51, 52]. The peaks located at 343 and 430 cm^{-1} correspond to the E_g symmetry mode, which represents an internal mode (i.e., bending of the MnO_6 octahedra). Moreover, the two highest peaks located at 550cm^{-1} for LSCMO11 and at 613, 662, and 655 cm^{-1} for LSCMO7, LSCMO9, and LSCMO13 nanocrystallites are attributed to the E_g bands, which are related to the vibration of oxygen in the MnO_6 octahedra. [53].

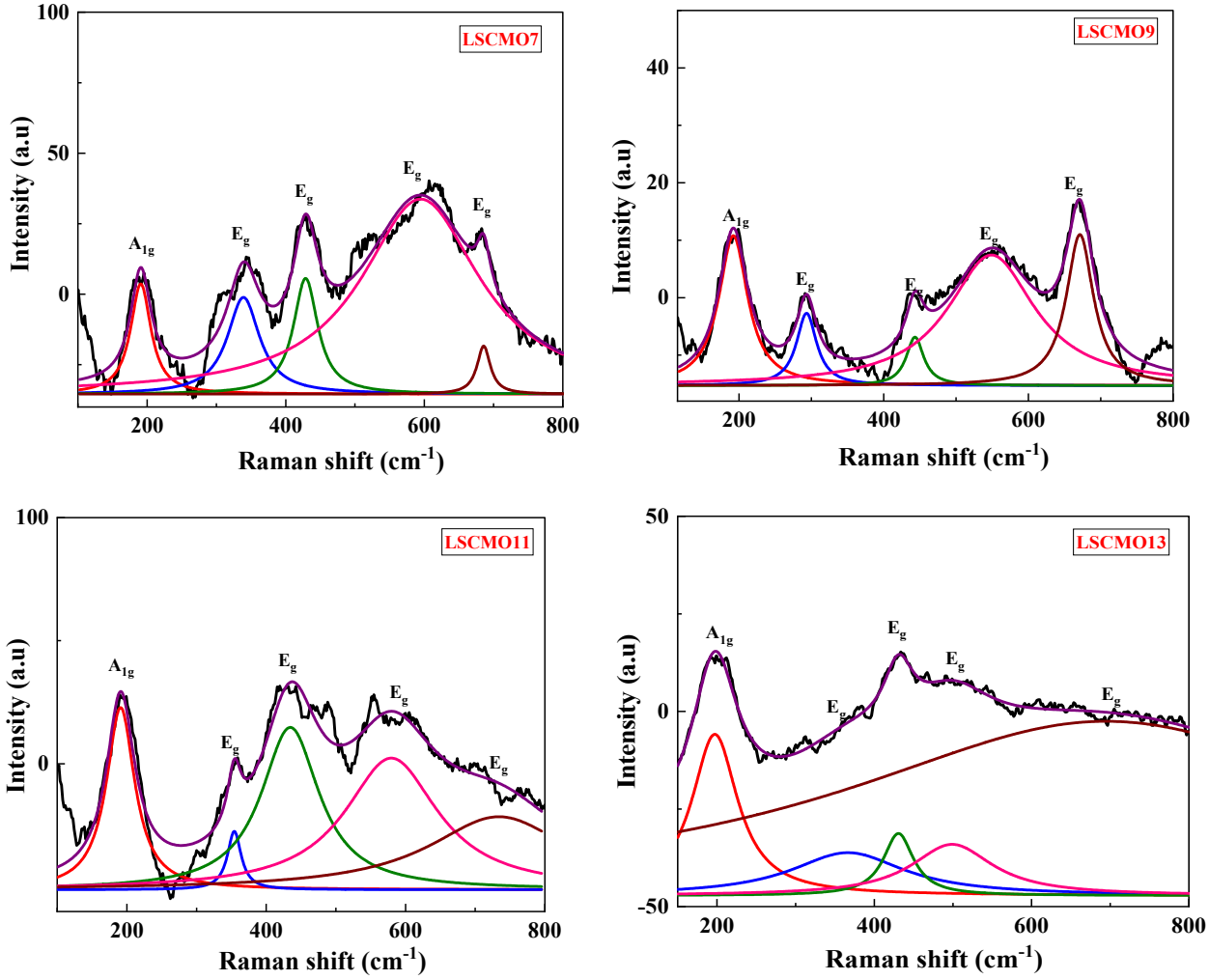

Figure 10. Deconvolution fitting of Raman spectra of LSCMO7, LSCMO9, LSCMO11, and LSCMO13 nanocrystallites

Table 4. Raman vibrational modes of LSCMO7, LSCMO9, LSCMO11, and LSCMO13 nanocrystallites.

Raman modes	LSCMO7	LSCMO9	LSCMO11	LSCMO13
$A_{1g}(cm^{-1})$	177	184	189	190
$E_g(cm^{-1})$	293	291	298	213
$E_g(cm^{-1})$	343	343	335	310
$E_g(cm^{-1})$	428	437	417	433
$E_g(cm^{-1})$	613	662	600	655

The position of Raman modes of all samples changes with annealing temperature can be observed from the Figure 11 and clearly shows that the A_{1g} mode is shifted from 177 to 190cm^{-1} (blue shift) with increase of annealing temperature from700 to 1300℃ and no significant change were observed for E_g symmetry modes (around 343 and 430 cm^{-1}). However, inverse effect was observed for the samples LSCMO11, and LSCMO13 in the E_g bands around 298 and 600cm^{-1}. From the Figure 11, it is evident that the Raman active phonon modes are greatly influenced by crystallite size.

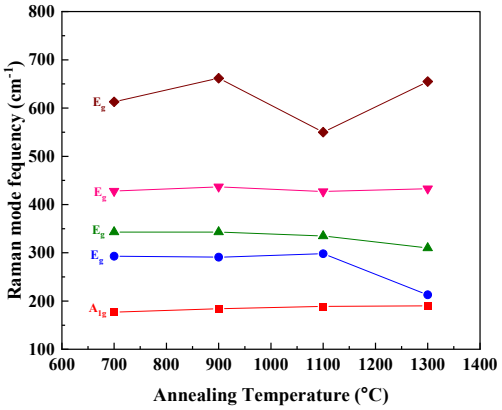

Figure 11. Annealing temperature dependence of Active Raman mode frequencies of $La_{0.7}Sr_{0.15}Ca_{0.15}MnO_3$ nanocrystallites

Magnetic Behaviour Analysis

Vibration sample magnetometer was used to measure the magnetic field dependence of magnetization of LSCMO7, LSCMO9, LSCMO11, and LSCMO13 nanocrystallites at room temperature, ranging from -1.5 to 1.5T, and corresponding local M-H hysteresis loops were displayed in Figure 12.

Figure 13 shows enlarged curves of M-H loops of all samples gives the values of the saturation magnetization (Ms), remanent magnetization (Mr), and coercive field (Hc) and observed that all samples exhibit ferromagnetic behaviour. Table 5 displays the characteristic parameters obtained from the local M-H hysteresis loops. The saturation magnetization (Ms), remanent magnetization (Mr), and coercive field (Hc) of all samples increase with the annealing temperature, indicating that the magnetic response increases with the increase in crystallite size.

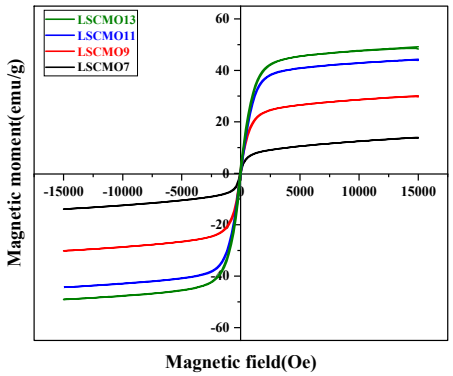

Figure 12. Variation of magnetic moment as function of Magnetic field of LSCMO7, LSCMO9, LSCMO11, and LSCMO13 nanocrystallites

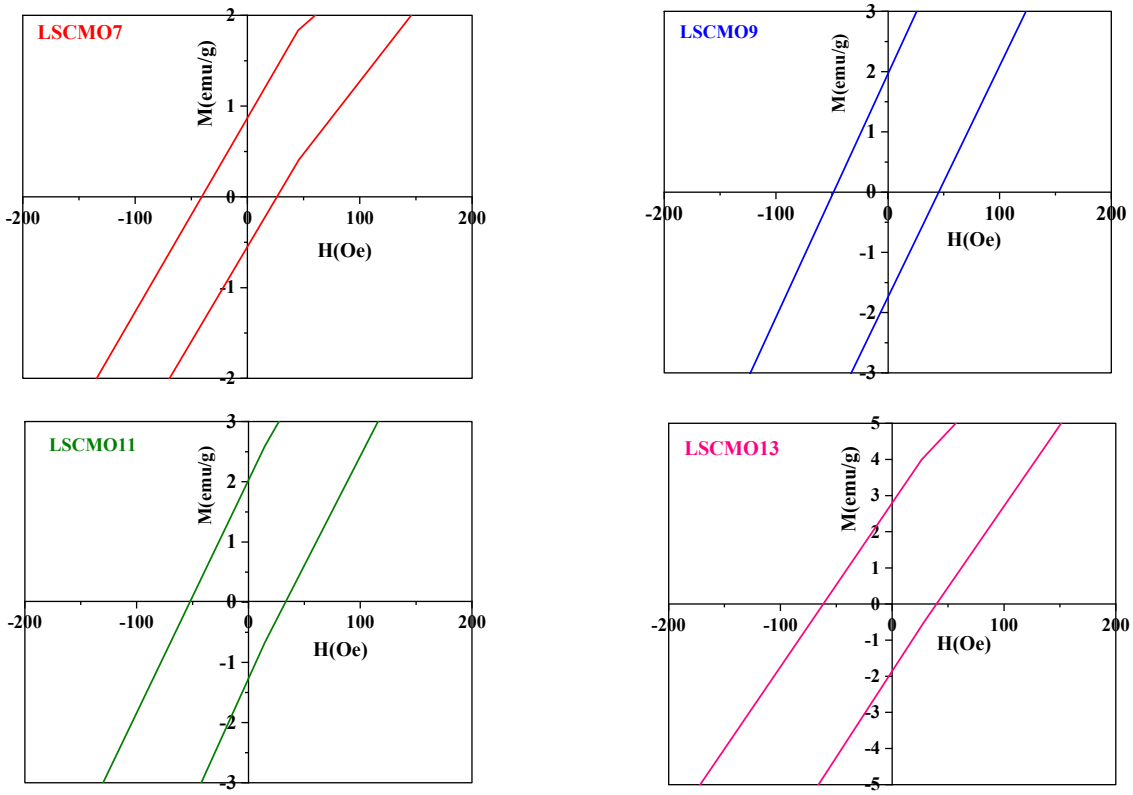

Figure 13. Enlarged curves of M-H loops of LSCMO7, LSCMO9, LSCMO11, and LSCMO13 nanocrystallites

Table 5. Magnetic parameters of LSCMO7, LSCMO9, LSCMO11, and LSCMO13 nanocrystallites.

Magnetic parameters	**LSCMO7**	**LSCMO9**	**LSCMO11**	**LSCMO13**
Saturation magnetization (M_s) (emu/g)	13.875	30.166	44.210	49.168
Remanent magnetization (M_r) (emu/g)	0.862	1.974	2.003	2.761
Coercive field (H_c) (Oe)	40.584	48.609	52.804	62.380

CONCLUSIONS

$La_{0.7}Sr_{0.15}Ca_{0.15}MnO_3$ nanocrystalline were effectively produced through combustion method and annealed at different temperatures to obtain various sizes of crystals and endorsed the phase formation of rhombohedral ($R\bar{3}c$) with no evidence of impurity peaks. The annealing temperature resulted in an increase in lattice parameters and crystalline size. The morphology and element composition were confirmed by SEM and EDX. FTIR main absorption band verified the presence of around 597cm^{-1} showed that LSCMO nanoparticles form a perovskite structure. This frequency shifted towards higher wave number to 613cm^{-1}(blue-shift) as the annealing temperature was increased, suggested that additional deformation of the MnO_6 octahedron. The results of the UV-vis spectroscopic analysis indicated that the LSCMO nanocrystallites were semiconductors with a broad band gap. As the size of the particles increased, the values of the optical band gap decreased from 3.51 eV to 3.25 eV. The Raman spectra of LSCMO showed that five vibration modes are formed around. The A_{1g} mode is shifted from 177 to 190 cm^{-1} (blue shift) with increase of annealing temperature from 700 to 1300°C. LSCMO nanocrystallites presents ferromagnetic properties, show increasing response with annealing temperature. Hence, the structural, optical, and magnetic properties of $La_{0.7}Sr_{0.15}Ca_{0.15}MnO_3$ nanocrystalline are significantly affected by the crystallite sizes.

ORCID

Mohd Abdul Shukur, https://orcid.org/0000-0003-3506-412X
Katrapally Vijaya Kumar, https://orcid.org/0000-0001-6160-8632
Gade Narsinga Rao, https://orcid.org/0000-0002-8229-8992

REFERENCES

[1] V. Franco, J.S. Blazqee, J.J. Ipus, J.Y. La, L.M. Moreno, and A. Conde, Prog. Mater, Sci. **93,** 112 (2018), https://doi.org/10.1016/j.pm atsci.2017.10.005
[2] V.K. Pecharsky, and K.A. Gschneidner Jr, J. Magn. Mag. Mater. **200,** 44 (1999), http://doi.org/10.1016/S0304-8853(99)00397-2
[3] T.D. Thanh, L.H. Nguyen, D.H. Manh, N.V. Chien, P.T. Phong, N.V. Khiem, L.V. Hong, and N.X. Phuc, Physica B: Condensed Matter. **407,** 145 (2012), https://doi.org/10.1016/j.physb.2011.10.006
[4] A. Gaur, and G.D. Varma, J Phys: Condens Matter. **18,** 8837 (2006), http://dx.doi.org/10.1088/0953-8984/18/39/014
[5] S. Zhao, X.-J. Yue, and X. Liu, Ceram. Int. **43,** 13240 (2017), http://dx.doi.org/10.1016/j.ceramint.2017.07.021
[6] U. Shankar, and A.K. Singh, The Journal of Physical Chemistry C, **119,** 28620 (2015), http://dx.doi.org/10.1021/acs.jpcc.5b08381
[7] W. Xia, L. Li, H. Wu, P. Xue, and X. Zhu, Ceram Int. **43,** 3274 (2017), http://dx.doi.org/10.1016/j.ceramint.2016.11.160
[8] N. Zaidi, S. Mnefgui, A. Dhahri, J. Dhahri, and E.K. Hlil, J. Alloys Compd. **616,** 378 (2014), https://doi.org/10.1016/j.jallcom.2014.07.113
[9] H. Nakatsugawa, M. Saito, and Y. Okamoto, Journal of Electronic materials, **46**, 3262 (2017), http://dx.doi.org/10.1007/s11664-017-5366-3
[10] Y. Tokura, Reports on Progress in Physics. **69**, 797 (2006), http://dx.doi.org/10.1088/0034-4885/69/3/R06
[11] C.B. Larsen, S. Samothrakitis, A.D. Fortes, A.O. Ayas, M. Akyol, A. Ekicibil, and M. Laver, Journal of Magnetism and Magnetic Materials, **498**, 166193 (2020), http://dx.doi.org/10.1016/j.jmmm.2019.166192
[12] M. K. Verma, N.D. Sharma, S. Sharma, N. Choudhary, and D, Singh, Materials Research Bulletin.**125,** 10813(2020), http://dx.doi.org/10.1016/j.materresbull.2020.110813
[13] S. Biswas, and S. Keshri, Journal of Materials Science: Materials in Electronics. **31**, 21896(2020). http://dx.doi.org/10.1007/s10854-020-04694-9
[14] L. Joshi, S. Rajput, and S. Keshri, Phase Transitions. **83**, 482 (2010), http://dx.doi.org/10.1080/01411594.2010.492466
[15] R.V. Helmholt, J. Wecker, and B. Holzapfel, Phys. Rev. Lett. **71**, 2331 (1993), https://doi.org/10.1103/PhysRevLett.71.2331
[16] K. Chahara, T. Ohno, and M. Kasai, Appl. Phys. Lett. **63**, 1990 (1993), https://doi.org/10.1063/1.110624
[17] S Jin, T.H. Tiefel, M. McCormack, R.A. Fastnacht, R.Ramesh, and L.H. Chen, Science, **264**, 413 (1994), https://doi.org/10.1126/science.264.5157.413
[18] D.H. Manh, P.T. Phong, T.D. Thanh, D.N.H. Nam, L.V. Hong, and N.X. Phuc, J Alloy Compd. **509,** 1373 (2011), https://doi.org/10.1016/j.jallcom.2010.10.104
[19] K. Navin, R. Kurchania, Ceram Int. **44,** 4973 (2018), http://dx.doi.org/10.1016/j.ceramint.2017.12.091
[20] M. Oumezzine, O. Pena, T. Guizouarn, R. Lebullenger, and M. Oumezzine, J. Magn. Magn. Mater. **324**, 2821 (2012), http://dx.doi.org/10.1016/j.jmmm.2012.04.017
[21] M. Rosic, L. Kljaljevic, D. Jordanov, M. Stoiljikovic, V. Kusigerski, V. Spasojevic, and B. Matovic, Ceram. Int. **41,** 14964 (2015), http://dx.doi.org/10.1016/j.ceramint.2015.08.041
[22] R. Von Helmolt, J. Wecker, B. Holzapfel, L. Schultz, and K. Samwer, Phys. Rev. Latt. **71**(14), 2331 (1993), https://doi.org/10.1103/PhysRevLett.71.2331
[23] M. Yamanaka, and N. Nagaosa, Phys B, **28,** 237 (1997), https://doi.org/10.1016/S0921-4526(97)00034-3
[24] Q.L. Fang, J.M. Zhang, and K.W. Xu, J. Magn. Magn. Mater. **349**,104 (2014), https://doi.org/10.1016/j.jmmm.2013.08.030
[25] A. Sundaresan, J.L. Tholence, A. Maignan, B. Raveau, E. Suard, and P. Border, J. Magn. Magn. Mater. **226-230**(1), 777 (2001), https://doi.org/10.1016/S0304-8853(00)01323-8

[26] G. Alejandro, M. Tovar, A. Butera, A. Caneiro, M.T. Causa, F. Prado, and R. Sánchez, Phys. B. **284-288(2),** 1408 (2000), https://doi.org/10.1016/S0921-4526(99)02571-5
[27] G.C. Rout, Nilima Parhi, and S.N. Behera, Phys. B. **404**, 2315 (2009), https://doi.org/10.1016/j.physb.2009.04.036
[28] M.H. Phan, S.C. Yu, and N.H. Hur, Appl. Phys. Lett. **86,** 072504 (2005), https://doi.org/10.1063/1.1867564
[29] W. Xia, K. Leng, Q. Tang, L. Yang, Y. Xie, Z. Wu, and X. Zhu, AIP Advances, **11**, 035007 (2021). https://doi.org/10.1063/5.0036723
[30] N.D. Lipham, G.M. Tsoi, and L.E. Wenger, IEEE Transactions on Magnetics, **43**, 3088 (2007). https://doi.org/10.1109/TMAG.2007.893850
[31] H. Wang, Z. Zhao, C.M. Xu, and J. Liu, Catal. Lett. **102**, 251 (2005). http://dx.doi.org/10.1007/s10562-005-5864-4
[32] W. Xia, H. Wu, P. Xue, and X. Zhu, Nanoscale Res. Lett. **13**, 135 (2018). https://doi.org/10.1186/s11671-018-2553-y
[33] S. Kumar, G. D. Dwivedi, S. Kumar, R. B. Mathur, U. Saxena, A. K. Ghosh, A. G. Joshi, H. D. Yang, and S. Chatterjee, Dalton Trans. **44,** 3109 (2015). https://doi.org/10.1039/C4DT03452J
[34] M.P. Reddy, R.A. Shakoor, and A.M.A. Mohamed, Mater. Chem. Phys. **177,** 346 (2016), https://doi.org/10.1016/j.matchemphys.2016.04.038
[35] Y. Liu, T. Sun, G. Dong, S. Zhang, K. Chu, X. Pu, H. Li, and X. Liu, Ceram. Int. **45,** 17467 (2019), https://doi.org/10.1016/j.ceramint.2019.05.308
[36] H.M. Pathan, J.D. Desai, and C.D. Lokhande, Appl. Surf. Science, **202**, 47 (2002), https://doi.org/10.1016/S0169-4332(02)00843-7
[37] M. Srivastava, A.K. Ojha, S. Chaubey, and A. Materny, Journal of Alloys and Compounds, **481**,515 (2009), https://doi.org/10.1016/j.jallcom.2009.03.027
[38] U. Kumar, D. Yadav, A.K Thakur, K.K. Srivastav, and S. Upadhyay, J. Therm. Anal. Calorim. **135**, 1987 (2018), https://doi.org/10.1007/s10973-018-7432-3
[39] F.R. Afje, and M. Ehsani, Materials Research Express, **5**, 045012 (2018), https://doi.org/10.1088/2053-1591/aaba51
[40] T.S. Moss, Proc. Phys. Soc. London, Sect. B, **63**, 167 (1950), https://doi.org/10.1088/0370-1301/63/3/302
[41] T.S. Moss, Phys. Status Solidi B, **131,** 415 (1985), https://doi.org/10.1016/1350-4495(94)90026-4
[42] P. Herve, and L.K.J. Vandamme, Infrared Phys. Technol. **35,** 609 (1994), https://doi.org/10.1016/1350-4495(94)90026-4
[43] W. Wang, and S.P. Jiang, Solid State Ionics. **177,** 1361 (2006), http://hdl.handle.net/20.500.11937/10875
[44] A.O. Turky, M.M. Rashid, A.M. Hassan, E.M. Elnaggard, and M. Bechelanyc, Phys. Chem. Chem, Phys. **19,** 6878 (2017), http://doi.org/10.1039/c6cp07333f
[45] V. Dediu, C. Ferdeghini, F.C. Matacotta, P. Nozar, and G. Ruani, Phys. Rev. Lett. **84,** 4489 (2000). https://doi.org/10.1103/PhysRevLett.84.4489
[46] L.M. Carr´on, A. de Andr´es, M.J. Mart´ınez-Lope, M.T. Casais, and J.A. Alonso, Phys. Rev. B. **66,** 174303 (2002). https://doi.org/10.1103/PhysRevB.66.174303
[47] X. Kong, J. Wang, Z. Zou, F. Long, and Y. Wu, J. Supercond. Novel Magn. **31,** 373 (2018), https://doi.org/10.1007/s10948-017-4217-z
[48] P.T. Phong, S.J. Jang, B.T. Huy, Y.I. Lee, and I.J. Lee, J. Mater. Sci. Mater. Electron. **24,** 2292 (2013), https://doi.org/10.1007/s10854-013-1092-7
[49] N.V. Minh, J. Phys. Conf. Ser. **187,** 012011 (2009), https://doi.org/10.1088/1742-6596/187/1/012011
[50] A. Dubroka, J. Humlíček, M.V. Abrashev, Z.V. Popović, F. Sapiña, and A. Cantarero, Phys. Rev. B **73,** 224401 (2006). https://doi.org/10.1103/PhysRevB.73.224401
[51] K. Daoudi, H. Alawadhi, S. El Helali, M. Boudard, Z. Othmen, M. Gaidi, M. Oueslati, and T. Tsuchiya, J. Phys. D: Appl. Phys. **50,** 395305 (2017), https://doi.org/10.1088/1361-6463/aa814f
[52] I. Krad, O. Bidault, N. Geoffroy, and M.E.L. Maaoui, Ceram. Int. **42,** 3751 (2016). http://dx.doi.org/10.1016/j.ceramint.2015.10.158
[53] A.E. Pantoja, H.J. Trodahl, A. Fainstein, R.G. Pregliasco, R.G. Buckely, G. Balakrishnan, M.R. Lees, and D. Mck. Paul, Phys. Rev. B. **63**, 132406 (2001). http://dx.doi.org/10.1103/PhysRevB.63.132406

ВПЛИВ РОЗМІРУ КРИСТАЛІТУ НА СТРУКТУРНІ, ОПТИЧНІ ТА МАГНІТНІ ХАРАКТЕРИСТИКИ НАНОКРИСТАЛІВ $La_{0.7}Sr_{0.15}Ca_{0.15}MnO_3$

Мохд Абдул Шукур[a,b], Катрапаллі Віджая Кумар[a], Гаде Нарсінга Рао[c]
[a]Кафедра фізики, Інженерний коледж університету JNTUH Раджанна Сірічілла, Аграхарам, район Раджанна Сірічілла, 505302, Телангана, Індія
[b]Кафедра фізики, Державний коледж мистецтв і науки SRR (автономний), Карімнагар, 505001, Телангана, Індія
[c]Кафедра фізики, Інститут технології та менеджменту Маррі Лаксман Редді, Дандігал, Хайдарабад, Телангана, Індія

Нанокристалічні манганіти $La_{0.7}Sr_{0.15}Ca_{0.15}MnO_3$ (LSCMO) були отримані в процесі спалювання та нагріті до різних температур відпалу (TA), щоб отримати кристаліти різного розміру. Картини рентгенівської дифракції (XRD) показали, що утворилася ромбоедрична структура з просторовою групою $R\bar{3}c$. Крім того, спостерігалося збільшення розміру кристалітів з 15,64 до 36,78 нм, коли температура (TA) зросла з 700°C до 1300°C. Мікрофотографії FESEM показали, що однорідні з пористістю. Спектри FTIR показали п'ять піків поглинання. Оптичний енергетичний проміжок нанокристалів LSCMO зменшується з 3,51 до 3,28 еВ із підвищенням температури відпалу, що показує, що наночастинки LSCMO є напівпровідниковими за своєю природою. Спектри комбінаційного розсіювання наночастинок LSCMO при кімнатній температурі демонструють значну залежність від температури відпалу. Коли раманівські моди аналізували відносно TA, було помічено, що коливальна фононна мода раманівського розсіювання нижче 200 $см^{-1}$ (A_{1g}) і чотири моди (Eg) в діапазоні 200-800 $см^{-1}$ показали значні зміщення та розширення, які були пов'язані з викривленням кисневої підґратки. Спостерігалися значні зміни як в інтенсивності, так і в напівмаксимумі повної ширини (FWHM) п'яти мод Рамана зі збільшенням температури відпалу. Магнітну поведінку за допомогою петлі M-H при кімнатній температурі виміряли магнітометром з вібраційним зразком і показали, що градація намагніченості насичення як функція температури відпалу. Таким чином, існує помітний вплив розміру кристалітів на оптичні та магнітні властивості нанокристалітів LSCMO.

Ключові слова: *розмір кристаліту; оптична заборонена зона; спектри FTIR; петля M-H; раманівські коливальні фонони*